Editors' Suggestion

Analog and Digital Phase Modulation and Signal Transmission with Spin-Torque Nano-Oscillators

A. Litvinenko,[1,*] P. Sethi,[1] C. Murapaka,[1] A. Jenkins,[2] V. Cros,[3] P. Bortolotti,[4] R. Ferreira,[2] B. Dieny,[1] and U. Ebels[1,†]

[1] *Univ. Grenoble Alpes, CEA, CNRS, Grenoble INP, Spintec, 38000 Grenoble, France*
[2] *International Iberian Nanotechnology Laboratory (INL), Braga, Portugal*
[3] *Unité Mixte de Physique CNRS, Thales, Université Paris-Sud, Université Paris-Saclay, Palaiseau, France*
[4] *THALES TRT, Palaiseau, France*

(Received 4 February 2021; accepted 19 May 2021; published 26 August 2021)

Spin-torque nano-oscillators (STNOs) are nanoscale devices with wide-band-frequency tunability. Their multifunctional rf properties are well suited to define schemes for wireless communications that use basic protocols for data transmission, such as amplitude-, frequency-, and phase-shift keying (ASK, FSK, and PSK, respectively). ASK and FSK are demonstrated for STNOs, but the implementation of PSK is more challenging because the STNO phase suffers from large fluctuations. Here, we introduce a special PSK technique for STNOs by combining their modulation and injection-locking functionality. The concept is validated using magnetic-tunnel-junction-based vortex STNOs for injection locking at $2f$ and $f/2$, showing phase shifts up to 0.70π rad and data-transmission rates up to 4 Mbit/s. Quadrature phase-shift keying and analog phase modulation are also implemented, where the latter is employed for voice transmission over a distance of 10 m. This demonstrates that the STNO's phase noise and output power meet the requested performances for operations in existing communication schemes.

DOI: 10.1103/PhysRevApplied.16.024048

I. INTRODUCTION

Wireless sensor networks (WSNs) are among the key enabling technologies of the Internet of things (IOT). In a WSN, a large number of nodes are interconnected and communicate with each other. Such applications require solutions that are wideband, compact, low cost, and autonomous. Recent advances of spin-torque nano-oscillator (STNO) performances [1,2] have led to active developments of communication and signal-processing systems [3–7], where STNOs are used as rf sources within transmitter-receiver blocks, exploiting their frequency tunability, nanoscale size, and multifunctionality. In a STNO, by way of compensation of damping, a spin-polarized dc injected through the magnetic stack induces steady-state oscillations of the free-layer magnetization [8]. STNOs are nonisochronous [9], i.e., their frequency depends on the amplitude of oscillation. This dependence provides tuning of the oscillation frequency via changing the input dc. Applying an additional rf signal (current or field) at the STNO input makes it possible to either injection lock the STNO to an external signal source [10–15] or to modulate the amplitude and frequency of the signal. So far, only frequency-shift keying (FSK) [16–22] and amplitude-shift keying (ASK) [3,4,18] have been demonstrated. However, the nanoscale dimensions of STNOs come at an expense of large phase noise [23,24], so that FSK and ASK signals generated by STNOs are not compatible with conventional communication protocols. One way around this would be to reduce the phase noise of the STNO by introducing a phase-locked loop (PLL). Such PLL operation has recently been demonstrated for STNOs of vortex or uniform magnetized states [25,26]. However, the reduction of phase noise happens only within the PLL filter bandwidth, which is limited by the signal-propagation delay in all PLL components. As an example, the PLL developed for vortex-state STNOs has a bandwidth of 4 MHz [25]. Another possibility to reduce phase noise and, thus, to stabilize the phase dynamics on short and long timescales, is to injection lock the STNO to an external rf current or field source [10–15]. In this case, the amplitude and frequency of the STNO's signal are fixed. However, it is possible to modulate the phase of the injection-locked STNO by changing the intrinsic (free-running) frequency. This opens the possibility to use a third basic concept of data communication, which is phase modulation (PM), including analog PM and digital phase-shift keying (PSK). The aim of this work is to first experimentally verify the principle of analog PM and digital PSK for STNOs, by

*litvinenkoan@gmail.com
†ursula.ebels@cea.fr

combining injection locking and modulation, and then to validate the principle by demonstrating voice transmission over distances of 10 m.

II. PRINCIPLE OF PM AND PSK FOR STNOS

The main idea of the PSK technique is that injection locking to a signal source, besides reducing the phase noise, provides a means to control the STNO phase, ϕ_{STNO} [27–30], with respect to the fixed reference phase, Φ_{source}. The corresponding phase difference in the injection-locked state, $\psi = \Phi_{\mathrm{source}} - N\Phi_{\mathrm{STNO}}$, is defined through an Adler-type equation, Eq. 1(a), that links ψ to frequency detuning, δ, Eq. 1(b), given by the mismatch of the free-running STNO frequency, f^0_{STNO}, and the source frequency, f_{source}. Equation (1) also considers injection locking at harmonics $N = 1, 2, 3, \ldots$, and at subharmonics [11,13] with $N = 1/2$, $1/3, \ldots$. The prefactor N in Eq. 1(a) for $N < 1$, arises from locking mechanisms that differ from the one for $N > 1$[27].

$$\psi(\delta) = \Phi_{\mathrm{source}} - N\Phi_{\mathrm{STNO}} = \begin{cases} \psi_0 + \arcsin\dfrac{\delta}{\Omega_N} \text{ for } N = 2, 3\ldots, \\ \psi_0 + N\arcsin\dfrac{\delta}{\Omega_N} \text{ for } N \le 1, \end{cases} \tag{1a}$$

$$\delta = f_{\mathrm{source}} - Nf^0_{\mathrm{STNO}}, \tag{1b}$$

$$\Delta\Phi_{\mathrm{STNOmax}} = \frac{\psi(\delta_{\max}) - \psi(-\delta_{\max})}{N} = \begin{cases} \pi/N \text{ for } N = 1, 2, 3\ldots, \\ \pi \text{ for } N = \dfrac{1}{2}, \dfrac{1}{4}, \ldots. \end{cases} \tag{1c}$$

In Eq. 1(a), ψ_o is the phase difference at zero detuning, $\delta = 0$, and Ω_N is the locking range that depends on the order N of synchronization, the locking forces, and STNO parameters [13,14,27]. It determines the maximum detuning, $\delta_{\max} = \pm\Omega_N$, for which the STNO remains injection locked. The full locking range is then $2\Omega_N$. When the STNO is locked, it oscillates at a frequency that is a multiple or integer fraction of the source frequency, $f_{\mathrm{STNO}} = f_{\mathrm{source}}/N$, with a phase, Φ_{STNO}, given by Eq. 1(a). A shift of Φ_{STNO} is achieved by detuning its free-running frequency, f^0_{STNO}, with respect to $\delta = 0$, while keeping f_{source} and Φ_{source} constant. The corresponding shift of the STNO phase is $\Delta\Phi_{\mathrm{STNO}}(\delta) = [\psi(\delta) - \psi_0]/N$. From Eq. 1(a), the maximum achievable STNO phase shift between $\delta_{\max} = +\Omega_N$ and $\delta_{\max} = -\Omega_N$ is $\Delta\Phi_{\mathrm{STNOmax}} = \pi$ for subharmonic injection locking and $\Delta\Phi_{\mathrm{STNOmax}} = \pi/N$ for harmonic injection locking, see Eq. 1(c). Based on this possibility of controlling the STNO phase, Φ_{STNO}, via the detuning of f^0_{STNO}, phase modulation of the STNO signal can be achieved by combining injection locking and modulation (see Fig. 1): (i) first a dc, I_{dc}, excites auto-oscillation at carrier frequency f^0_{STNO}; (ii) a rf signal, V_{source}, at frequency $f_{\mathrm{source}} = Nf^0_{\mathrm{STNO}}$ and $\delta = 0$ is used to injection lock the STNO; and (iii) a rf modulation signal, V_{mod}, is used to modulate the STNO free-running frequency, f^0_{STNO}, and through this the detuning, δ, resulting in a modulation of the STNO phase, Φ_{STNO}. Employing this principle, we demonstrate here digital binary phase-shift keying (BPSK), quadrature phase-shift keying (QPSK), and analog PM, which are used for wireless voice transmission using conventional receiver blocks.

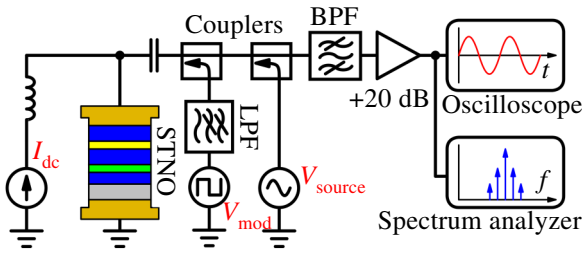

FIG. 1. Schematic of the electrical setup for digital PSK and analog PM using STNOs.

III. EXPERIMENTS AND RESULTS

The experimental setup is shown in Fig. 1. A dc source (Keithley 2401) is used for signal generation, a signal generator (Agilent E8257D) is used for injection locking, and a waveform generator (Tektronix AWG4162) is used for modulation. The two rf signals are injected via couplers to separate the STNO input and output signals. The phase-modulated STNO output signal is filtered by a band-pass filter (BPF) within a bandwidth of 50 MHz around a central frequency of 300 MHz and amplified by 20 dB using a commercial amplifier. For the PSK and PM experiments, magnetic tunnel junction (MTJ)-based vortex-state nano-oscillators are chosen, since they demonstrate the capability of perfect injection locking to an external signal source [13]. The MTJ vortex STNOs are realized by the International Iberian Nanotechnology Laboratory (INL). Their composition is as follows: Ta(5)/Cu − N(50)/Ta(5)/Cu − N(50)/Ta (5) / Ru(5)/Ir − Mn(6)/$CoFe_{30}$(2.6)/Ru (0.85) /$CoFe_{40}B_{20}$(1.8)/ MgO/VFL/Ta(10)/Cu − N(30)/Ru(7) (thicknesses in nm), where VFL is the vortex-state free layer, $CoFe_{40}B_{20}$(2.0)/ Ta(0.2)/Ni-Fe(7). Here, results for two devices of 370 nm in diameter with similar dynamic and static characteristics ($R_{\mathrm{STNO}} \approx 40$ Ohm, tunnel magnetoresistance (TMR) $\approx 150\%$, and resistance-area (RA) $\approx 4.5\ \Omega\ \mu\mathrm{m}^2$) are presented. The STNO output-voltage signal, V_{STNO}, is analyzed by a spectrum analyzer to deduce the STNO frequency, f_{STNO}; linewidth, Δf; and power, P, of the free-running, injection-locked, and modulated states, as well as

by a real-time oscilloscope in single-shot mode to register time traces. From the analysis of the time traces, using the Hilbert transform, the STNO phase, Φ_{STNO}, is extracted in the free-running, injection-locked, and phase-modulated state, similar to previous studies [13,15,20,22–24,31]. For injection locking as well as PSK and PM, the free-running oscillator frequency is set to $f^0_{\mathrm{STNO}} = 300$ MHz, using a dc of $I_{\mathrm{dc}} \approx 9.75$ mA and an out-of-plane field of $H \approx 2.5$ kOe. The corresponding linewidth and power are $\Delta f = 250$ kHz and $P = 0.25$ μW. Figure 2 shows the results for injection locking at $N = 2$, using a sinusoidal rf signal with $f_{\mathrm{source}} = 2f^0_{\mathrm{STNO}} = 600$ MHz and a power level of P_{source}. Figure 2(a) shows an example for $P_{\mathrm{source}} = -3$ dBm. Upon varying the free-running STNO frequency, $f^0_{\mathrm{STNO}}(I_{\mathrm{dc}})$, via I_{dc}, the STNO is locked to the source (i.e., $f_{\mathrm{STNO}} = 0.5 f_{\mathrm{source}}$) over a dc range of $2\Delta I_{\mathrm{lock}} \approx 0.5$ mA, which corresponds to a locking range of $2\Omega_N(I_{\mathrm{dc}}) \approx 2.6$ MHz. Over this range, the STNO linewidth, see Fig. 2(a) (blue line), drops below the resolution bandwidth (RBW) of the spectrum analyzer, set to RBW = 50 kHz for fast data processing. It is checked that the actual STNO linewidth in the locked state is close to the linewidth of the external signal source of about 1 Hz. In Fig. 2(b), we show the corresponding Arnold tongue P_{source} vs I_{dc}. The locking range expands with increasing rf power. P_{source}. The corresponding phase noise is shown in Fig. 2(c) for a rf power of -3 dBm and three different values of detuning, and the corresponding instantaneous phase dynamics is shown in Fig. 2(d). For large detuning beyond the locking range, point (1), the oscillator is unlocked and the phase is free, leading to a random walk of the instantaneous phase, which is reflected in large phase fluctuations in the time domain and a $1/f^2$ dependence in the phase noise [red curves, Figs. 2(c) and 2(d)]. At detuning values close to the locking-range boundary [point (2) near the red area in the Arnold tongue], the phase noise starts to flatten off below a roll-off frequency called here f_p [see Fig. 2(c)]. The instantaneous phase is partially locked but suffers from occasional phase slips [15], as reflected in the increasing phase noise with a slope of $1/f^2$ at offset frequencies below f_{corner} (blue curves). For zero detuning, point (3), and detuning within approximately 80% of the locking range, $-0.8\ \Omega_N \lesssim \delta \lesssim 0.8\ \Omega_N$, phase slips are absent in the STNO phase (red curve) within the time window of

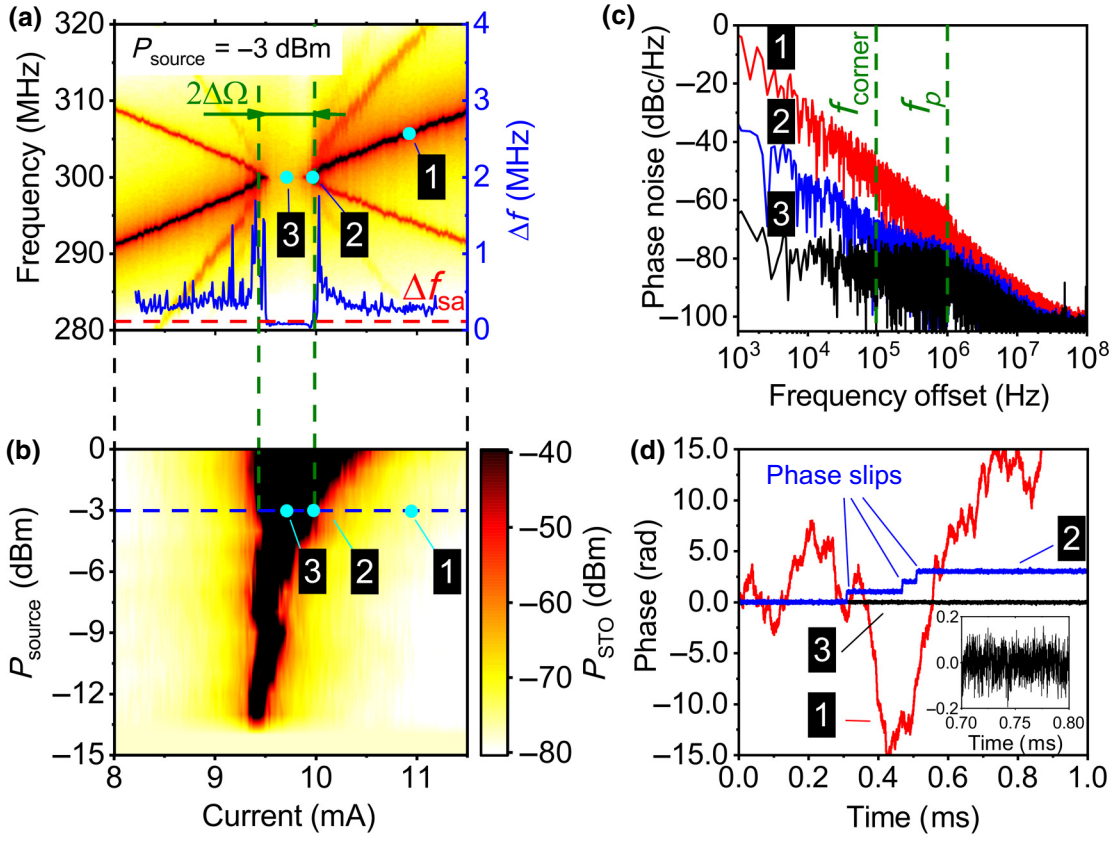

FIG. 2. $2f$ injection locking of the vortex-state STNO using a rf source of constant frequency $f_{\mathrm{source}} = 600$ MHz. (a) STNO spectrum and linewidth, Δf (blue line), vs I_{dc} at $P_{\mathrm{source}} = -3$ dBm. (b) Arnold tongue as a function of input power, P_{source}, and dc. (c) Phase noise and (d) corresponding time evolution of the STNO phase, Φ_{STNO}, for three different current values, I_{dc}, corresponding to three different states: (1) unlocked free-running STNO ($I_{\mathrm{dc}} = 11$ mA); (2) partially locked STNO ($I_{\mathrm{dc}} = 10$ mA) with phase slips; (3) injection locked STNO ($I_{\mathrm{dc}} = 9.75$ mA). Inset in (d) shows an enlarged scale of STNO phase vs time for point (3).

measurements (1 ms). The phase noise becomes flat in the range of offset frequencies below f_p (black curves). This behavior is consistent with that in Ref. [13]. It is in this area of the Arnold tongue with zero phase slips (perfect locking) where phase modulation has to be carried out.

We demonstrate BPSK for injection locking at $N = 2$ (called here $2f$ locking, with $f_{source} = 600$ MHz) and $N = 1/2$ (called here $f/2$ locking, with $f_{source} = 150$ MHz), keeping all other parameters as described above ($P_{source} = -3$ dBm, $I_{dc} \approx 9.75$ mA, $f^0_{STNO} = 300$ MHz). After injection locking, a time-varying modulation signal of peak-peak amplitude V_{mod} and with modulation frequency f_{mod} is added to the STNO in the form of a square-wave pattern. V_{mod} is limited to 12 mV ($2f$) and 8 mV ($f/2$), such that the detuning remains within 80% of the locking range, $\delta \cong 0.8\ \Omega_N$, to avoid phase slips. With this, the theoretically [see Eq. 1(a)] achievable maximum of the phase shift is expected to be $\Delta\Phi_{STNO} \approx 0.3\pi$ in the case of $2f$ and $\Delta\Phi_{STNO} = 0.6\pi$ in the case of $f/2$ injection locking. For larger values of V_{mod}, stochastic phase slips of Φ_{STNO} will occur, see Fig. 2(d) (trace 2). The results are summarized in Fig. 3, showing the time traces of the instantaneous STNO phase, Φ_{STNO} (red lines), as well as the modulation signal (black lines) for different amplitudes, V_{mod}, and modulation frequencies, f_{mod}. Figure 3(a) gives an example for $2f$ injection locking with $V_{mod} = 6$ mV and $f_{mod} = 500$ kHz. It can be clearly seen that Φ_{STNO} follows the input signal and that the phase shift is $\Delta\Phi_{STNO} \approx 0.16\pi$ rad. This value is increased to $\Delta\Phi_{STNO} \approx 0.29\pi$ rad when increasing V_{mod} to its maximum value of 12 mV, Fig. 3(b). This value of $\Delta\Phi_{STNO}$ is close to the predicted STNO phase shift of $0.3\ \pi$. As stated above, the maximum achievable phase shift is expected to be 2 times larger for $f/2$ than that for $2f$ locking. Figure 3(c) shows an increased phase

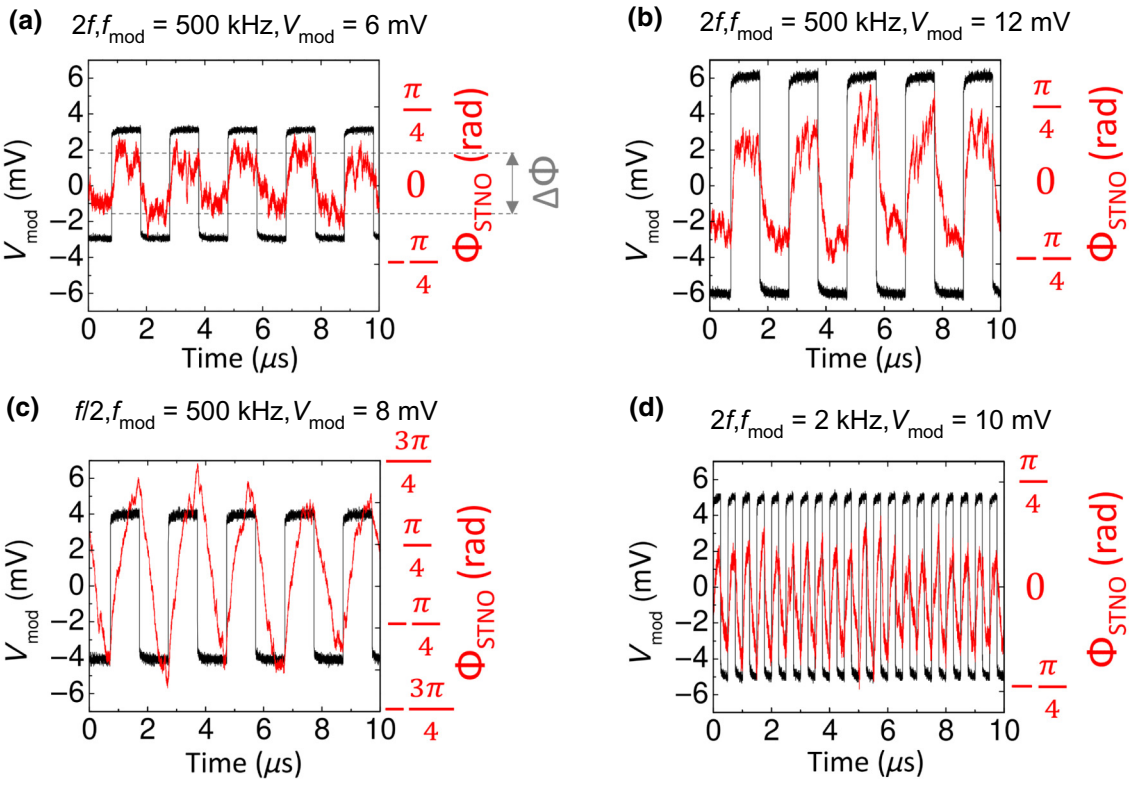

(e)

Nf	2*f*	2*f*	2*f*	2*f*	*f*/2	*f*/2	*f*/2	*f*/2
V_{mod} (mV)	6	10	12	10	4	6	8	6
f_{mod} (kHz)	500	250	500	2000	500	250	500	2000
$\Delta\Phi_{STNO}$ (rad)	0.16 π	0.24 π	0.29 π	0.19 π	0.35 π	0.67 π	0.70 π	0.19 π

FIG. 3. Demonstration of BPSK at $2f$ and $f/2$ injection locking using $P_{source} = -3$ dBm for different parameters of the binary modulation signal V_{mod} and f_{mod}. Time traces of the instantaneous STNO phase Φ_{STNO} (red) and modulation signal V_{mod} (black) are shown. Values of Nf, f_{mod}, and V_{mod} are (a) $2f$, 500 kHz, 6 mV; (b) $2f$, 500 kHz, 12 mV; (c) $f/2$, 500 kHz, 8 mV; (d) $2f$, 2 MHz, 10 mV. (e) Table for maximum phase shift, $\Delta\Phi$, achieved at different values of V_{mod} and f_{mod}.

shift of $\Delta\Phi_{STNO} \approx 0.8\pi$ rad for $f/2$ injection locking at $V_{mod} = 8$ mV and $f_{mod} = 500$ kHz. In Fig. 3(e), we summarize the phase shift for different measurement conditions. $\Delta\Phi_{STNO}$ increases with V_{mod} as long as f_{mod} is below the amplitude relaxation frequency, f_p [9,15,20,22,32,33]. In this device, f_p for the $2f$ locking regime is 1 MHz, which is typical for vortex STNOs [24]. As can be seen from Fig. 3(e), upon increasing f_{mod} from 250 kHz to 2 MHz, the amplitude of phase oscillations, $\Delta\Phi_{STNO}$, drops much more significantly in the case of $f/2$ locking than that for the $2f$ locking regime [Fig. 3(d)]. This is explained by the difference in f_p frequency for each synchronization regime and is similar to that shown in Ref. [13].

The results shown in Fig. 3 clearly demonstrate the BPSK scheme for STNOs where the phase follows the input signal within the limits discussed. Since the STNO phase is a continuous function of detuning of its free-running frequency, f^0_{STNO} [Eq. (1)], more phase states can be obtained to encode data, thus increasing the data-transmission capacity and channel efficiency. Here, we demonstrate four-level QPSK and continuous analog PM. Accommodating more phase states in the total phase shift, $\Delta\Phi_{STNO}$, reduces the signal-to-noise ratio. Therefore, we demonstrate QPSK and PM at a lower modulation rate of 10 kHz. In addition, a low-pass numerical filter with a cut-off frequency of 300 kHz is applied to the instantaneous phase signal to filter out high-frequency noise. Figure 4(a) shows the QPSK modulation of Φ_{STNO} with four distinguishable levels, and Fig. 4(b) shows the analog PM using a sawtooth signal for V_{mod}. As can be seen, Φ_{STNO} is continuous and close to linear with a maximum phase shift of $\Delta\Phi_{STNO} \approx 0.22\pi$ rad, which corresponds to the expected value when using $V_{mod} = 8$ mV (chosen to stay well within the Arnold tongue and avoid phase slips on a millisecond timescale).

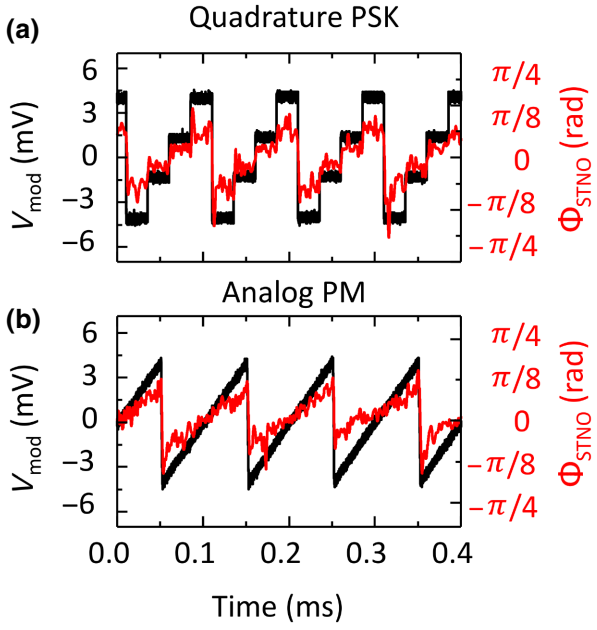

FIG. 4. Demonstration of (a) QPSK and (b) analog PM using a sawtooth signal for $2f$ injection locking with $P_{source} = -3$ dBm and parameters of the modulation signal of $V_{mod} = 8$ mV and $f_{mod} = 10$ kHz. Time traces of the instantaneous STNO phase, Φ_{STNO} (red), and modulation signal, V_{mod}, are shown (black).

The modulation protocols of BPSK, QPSK, and analog PM demonstrate the versatility of STNO modulation, which will be of interest for different types of applications. While BPSK and QPSK are used for digital data transfer at higher data rates, analog PM will be of interest for transmission of analog data, such as sensor readings.

IV. SIGNAL TRANSMISSION WITH STNOS

The possibility of real-time analog data transmission is shown in the following example of analog voice transmission. The scheme used for voice transmission is shown in Fig. 5, where the transmitter part is similar to that in Fig. 1, replacing the waveform generator for modulation by a microphone. For injection locking, the frequency of the external source V_{source} was chosen to be half of the intrinsic STNO frequency, since $f/2$ locking leads to a maximum phase modulation of $\Delta\Phi_{STNO} = \pi$ and, thus, to a better signal-to-noise ratio (SNR). Microphone amplification is chosen so that the maximum amplitude of the phase modulation is within 30% of the full locking range to avoid phase slips on long timescales of tens of seconds. The total phase change, therefore, is approximately $\Delta\Phi_{STNO} = 0.3\pi$ rad. To demonstrate the potential, the voice-modulated signal is then directly fed to a 2-dBi emitter antenna for transmission, without amplification (i.e., the 20-dB amplifier of Fig. 1 is removed and the power that arrives at the transmitter antenna is −40 dBm). The signal is received by a 2-dBi receiver antenna, positioned at a distance of 10 m from the transmitter. A general-purpose register transfer logic (RTL) software-defined radio (SDR) receiver based on RTL2832U and R820T [34] chips is used for demodulation of the received phase-modulated signal.

The SDR receiver is controlled by a personal computer (PC) program (SDRSharp [35]) that produces an audible decoded signal. A real-time video with an audible soundtrack can be found online within the Supplemental Material [36]. The transmitted signal is visualized in the form of a frequency-time spectrogram, which is also shown in Fig. 6(a). When there is no input at the microphone, only the injection-locked carrier signal is seen. From $t = 1$ to 9 s the microphone is switched on and the voice transmission starts, generating sidebands on the carrier that are clearly seen in the spectrogram of Fig. 6(a). Notably, the SDR receiver has preamplifiers, so that the amplitude of the carrier of the received signal becomes −10 dBm. For comparison, we show in Fig. 6(b) (red line) the power

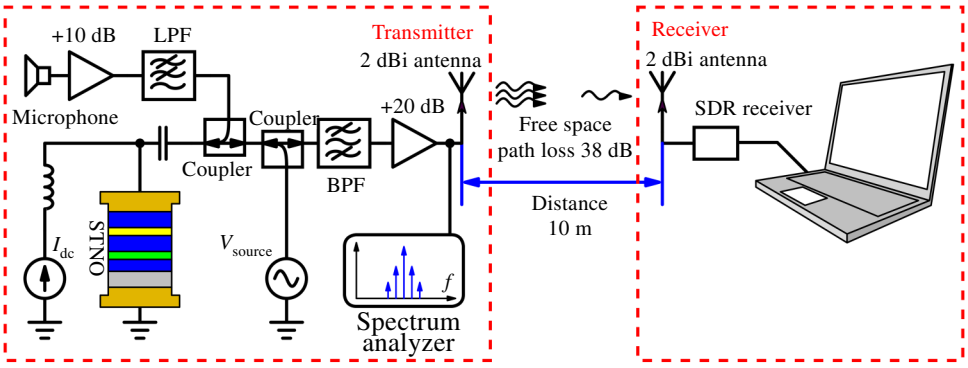

FIG. 5. Schematics of the benchtop system used for wireless voice transmission. BPF is a bandpass filter with a band of 50 MHz and a central frequency of 300 MHz. LPF is low-pass filter with a cutoff frequency of 20 kHz.

spectrum (PS) for a BPSK signal that corresponds to the time traces of Fig. 3(a). This experiment on voice transmission using analog phase modulation is an important proof of concept for the direct implementation of STNOs in standard communication systems, demonstrating that the STNO power of 0.25 μW is sufficient for communication over distances of several meters and that STNOs are compatible with standard rf system components. In the following, we further discuss the performances of the PSK and PM technique.

Some pertinent parameters that define the application area of a wireless communication system are the maximum achievable data rate (depending on the modulation technique and on the SNR), the occupied bandwidth, and the maximum achievable distance of communication. Wireless sensor networks present the biggest share of all wireless connected objects, which includes the IOT; their application range is large and varied, and wireless communication distances can be anything between short range [<1 m, such as wireless body area networks (WBAN)] and long range [100–10 km, such as low-power wide-area network (LPWAN)]. Based on the experimental results, we assess the SNR for analog phase modulation (e.g., voice transmission) and digital binary phase-shift keying, as well as the bit error rate (BER) and maximum data-transmission rate (MDR) for BPSK. From this, it is possible to estimate the maximum achievable distance of communication for a given power level and channel bandwidth. Details and equations used are given in the Supplemental Material [36]. Here, we present only the main ideas and results. For all three parameters, SNR, BER, and MDR, we obtain the power levels of the main peak, first sideband, and noise floor from the PS plot in Fig. 6(b). As an example, the power of the main peak of the BPSK signal is $A_0 = -15$ dBm (including 20 dB amplification). This corresponds well to the (nonamplified) power of 0.25 μW measured in the free-running state. The second piece of information is the ratio of the power of the first sideband, A_1, to that of the carrier, A_0, which in our case of BPSK is $A_{0\mathrm{PSK}}/A_{1\mathrm{PSK}} = 16$ dB and for PM is 10 dB due to the use of $f/2$ synchronization. Using these values, the sensitivity of the SDR receiver employed in the experiment, as well as the free-space path loss [37], we calculate the SNR, BER, and MDR at the transmitter and receiver [36]. We start with the SNR of the PM and BPSK, which are shown in Fig. 7.

In the case of the PM experiment, the SNR at the transmitter output is calculated to be $\mathrm{SNR}_T = 33$ dB [36], which is a very high value [horizontal dashed line in Fig. 7(a)]. At a distance of 1.3 m [vertical dashed line in Fig. 7(a)], the level of the PM signal at the position of the receiver drops (due to the FSPL), such that the receiver noise starts

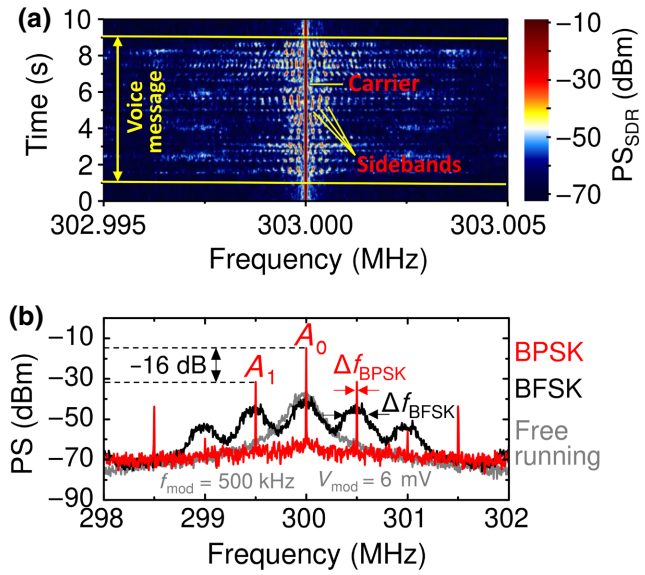

FIG. 6. (a) Frequency-time spectrogram at the SDR receiver for transmission of the following message: "Demonstration of voice transmission using phase modulation of spin-torque nano-oscillators". Parameters are described in the text. During voice transmission, sidebands are generated, as indicated. (b) Comparison of PS plots of the STNO output voltage after amplification of 20 dB, as measured on a spectrum analyzer within a RBW of 1 kHz for the free-running STNO (gray curve), binary FSK modulated signal (black curve), and binary PSK signal (red curve). BPSK data are taken for injection locking at $2f$ with $P_{\mathrm{source}} = -3$ dBm, and amplitude of the modulation signal for binary frequency shift keying (BFSK) and BPSK signal is $V_{\mathrm{mod}} = 6$ mV. PS corresponds to the power within the resolution bandwidth set to RBW $= 1$ kHz.

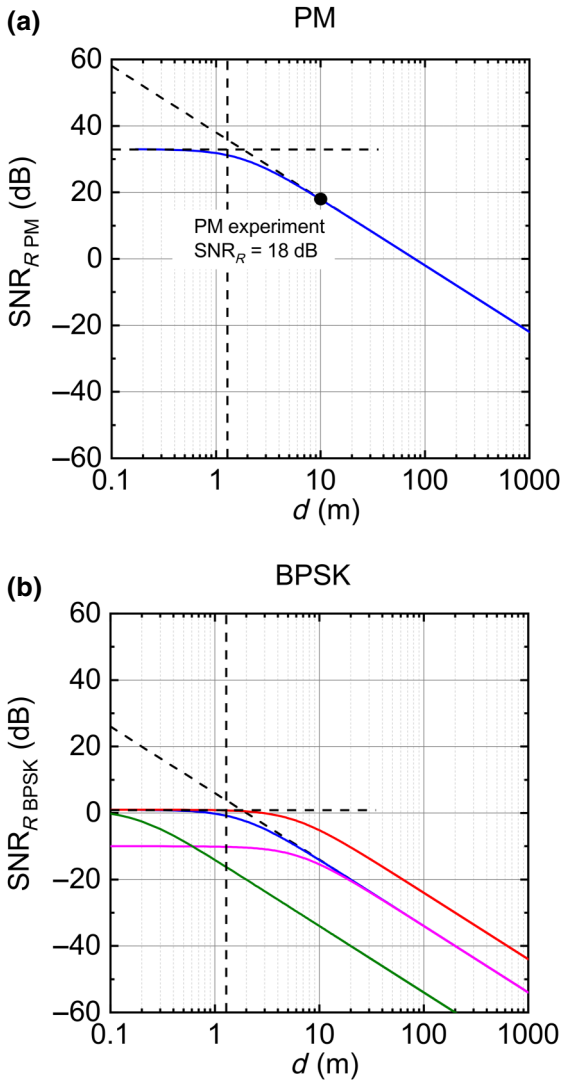

FIG. 7. Signal-to-noise ratio for different parameters for (a) analog PM and (b) digital BPSK phase modulation as a function of distance between emitter and receiver. Horizontal dashed lines are SNR values at transmitter output. Vertical dashed lines correspond to the maximum distance for which the contribution of the internal STNO noise is larger than that from the receiver noise and, therefore, determines the SNR. Diagonal dashed lines correspond to a reduction of SNR due to free space path loss (FSPL) [36,37]. Evaluation of SNR for (a) PM signal using carrier frequency of 300 MHz, amplification of 0 dB, and bandwidth of 5 kHz and (b) for a BPSK signal for different parameters of modulation bandwidth, additional amplification, and carrier frequency; blue curve, carrier frequency 300 MHz, amplification 0 dB, bandwidth 2 MHz; green curve, carrier frequency 3 GHz, amplification 0 dB, bandwidth 2 MHz; red curve, carrier frequency 3 GHz, amplification 30 dB, bandwidth 2 MHz; magenta curve, carrier frequency 3 GHz, amplification 30 dB, bandwidth 20 MHz.

to influence the total signal, SNR_{RPM} [diagonal dashed line in Fig. 7(a)]. At a distance of 10 m, for which the voice transmission experiment is done, the SNR_{RPM} drops down to 18 dB [black dot in Fig. 7(a)], which is still enough for 100% speech recognition [38]. In the case of BPSK, following the same analysis, the SNR at the transmitter is slightly larger than zero [horizontal dashed line in Fig. 7(b)] and, similar to PM, starts to drop significantly above 1.3 m [vertical dashed line Fig. 7(b)]. The reduced value of the transmitter SNR for BPSK is due to the larger channel bandwidth, which is 2 MHz for BPSK and 5 kHz for PM.

From the estimates of vortex devices presented here with $f = 300$ MHz, we can now make a prediction for devices emitting at higher frequencies, such as $f = 3$ GHz (realized, for instance, using uniformly magnetized STNOs). Considering the same generated power level of carrier A_0 and bandwidth of 2 MHz, the SNR starts to drop at a distance of 0.1 m [green curve in Fig. 7(b)]. However, using an additional amplification of 30 dB, it is possible to increase the distance of data transmission up to 5 m, keeping the $\mathrm{SNR} > 0$ [red curve in Fig. 7(b)]. The bandwidth (or modulation frequency) of 2 MHz chosen here is relatively low, and many applications target much higher modulation rates. In principle, this is possible for uniform-state STNOs, for which modulation frequencies up to 200 MHz [22] are demonstrated. However, an increase of modulation frequency means an increase of the channel bandwidth and using only a 5 times increase of the channel bandwidth of 10 MHz [pink curve in Fig. 7(b)], leads to a drop of the SNR at the transmitter to -7 dB, making data transmission at this rate impossible [39]. This result calls for some comments on how to increase the SNR at the transmitter side to allow larger modulation bandwidths. An increase of the free-running STNO power at a constant linewidth (i.e., at constant phase-noise level) will not be sufficient. The STNO phase-noise level itself needs to be reduced to reduce the phase-noise level at low offset frequencies in the synchronized state. This can be achieved by using not a single STNO, but an array of synchronized STNOs [40,41]. For example, to profit from the maximum modulation frequency of 200 MHz for uniform STNOs, the SNR of a STNO BPSK-modulated signal has to be improved by $10\log_{10}(200\ \mathrm{MHz}) - 10\log_{10}(2\ \mathrm{MHz}) = 20$ dB. Each 3 dB of the phase-noise improvement requires doubling of the number of synchronized oscillators. Therefore, to improve the SNR by 20 dB, one needs to synchronize $2^{20/3} \approx 100$ oscillators, which seems to be realistic, taking into account that synchronization of up to 64 spin Hall nano-oscillators has already been experimentally demonstrated [40]. Another way to improve the noise properties in the synchronized state is to use higher orders of injection locking of $2f$, $3f$, $4f$, etc. [13]. The use of higher orders of injection locking leads to a narrowing of the separation between dynamic locking barriers and, therefore, reduces the amplitude of the STNO phase fluctuations within the barrier.

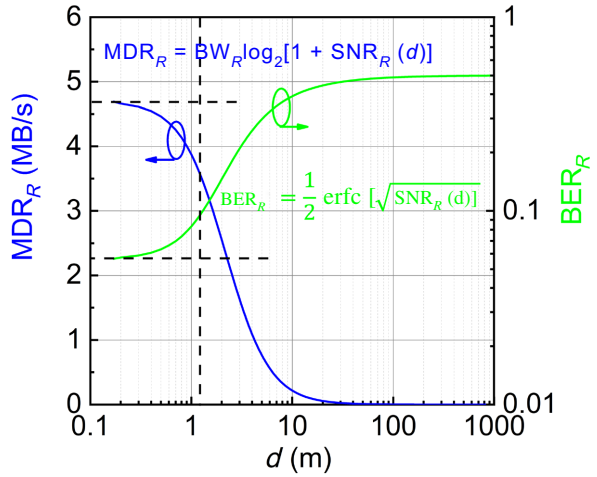

FIG. 8. MDR (left scale) and BER (right scale) for BPSK signal as a function of distance. Horizontal dashed lines show levels of MDR and BER at the transmitter. Vertical dashed line shows the distance at which SNR at the receiver drops by 3 dB. Blue and green lines correspond to equations for MDR and BER at the receiver, respectively.

Another important evaluation parameter for data transmission using BPSK is the MDR and BER [36]. These parameters directly depend on the SNR_R at the receiver.

As can be seen from Fig. 8, the level of the BER is acceptable, starting from the transmitter at a level of 0.0563 and reaching 0.1 at a distance of 1.3 m. This is expected to be enough for data communication using conventional protocols with error-correction procedures. From these estimations, we conclude that an acceptable SNR and BER can be achieved to transmit data without significant degradation of the MDR up to a distance of 1.3 m at a rate of 3.5 Mb/s (Fig. 8). Hence, the main area of application of STNOs will be for short-distance communication, such as in wireless communication networks.

V. SUMMARY

In summary, we demonstrate a concept to realize digital phase-shift keying and analog phase modulation with spin-torque nano-oscillators. This concept combines the three STNO rf functionalities of (i) signal generation via a dc; (ii) injection locking to a rf source at a constant source frequency; and (iii) modulation of the intrinsic (free-running) STNO frequency, f^0_{STNO}, via a modulation voltage, V_{mod}. The resulting frequency detuning induces a modulated phase shift in the STNO output signal, where the total phase shift increases with the modulation voltage, V_{mod}, given that detuning is smaller than the locking range. The concept is demonstrated for vortex-state STNOs, for which a phase shift of 0.70π rad is achieved for injection locking at the subharmonic $f/2$. This is close to the recommended value given by the IEEE standards [42] for the BPSK technique. We achieve maximum data rates of 4 Mbit/s for BPSK and demonstrate that (taking into account state-of-the-art parameters of vortex and uniform STNOs) data transmission at such rates is feasible for distances of up to around 1 m. We find that, for the BPSK technique exploiting injection locking, the achieved MDR of 4.7 Mb/s is limited primarily by the SNR of the STNO signal in the injection-locked state. The main limitation of the SNR and, thus, the MDR and BER is the level of STNO phase noise in the synchronized state [39]. Given that the SNR can be sufficiently improved using different approaches, such as synchronization [39] and higher-order injection locking [13], the maximum data rate can then be increased up to a rate determined by the amplitude relaxation frequency, f_p, or even beyond if using the rf field for modulation, as proposed in Ref. [31].

We also implement analog PM (continuous modulation) of vortex STNOs and demonstrate voice transmission over a distance of 10 m using commercial receivers. The achieved results demonstrate that the performances of STNOs, in terms of output power and SNR, are compatible with existing rf components and demodulation electronics for short-range WSN communication systems. For full integration within a CMOS, it will be of interest to combine the PSK technique demonstrated here for STNOs with the PLL operation of STNOs demonstrated earlier [25,26]. The idea is to use one STNO stabilized by a PLL as a frequency-tunable rf source that will replace the external signal source to lock a second STNO for PSK and PM modulation. This would be the first step towards a spintronics-based compact and effective communication scheme for WSN applications that should open the path to further spintronics-based microwave circuits.

Data that support the plots within this paper and other findings of this study are available from the corresponding authors upon reasonable request.

ACKNOWLEDGMENTS

The authors acknowledge Dmitry Postnov for fruitful discussions on phase detuning of an externally synchronized oscillator. Financial support is acknowledged from the French space agency CNES, Enhanced Eurotalent program, from ERC MagiCal Grant. No. 669204, and from ANR-SPINNET Grant No. ANR-18-CE24-0012.

[1] S. Tsunegi, K. Yakushiji, A. Fukushima, S. Yuasa, and H. Kubota, Microwave emission power exceeding 10 μW in spin torque vortex oscillator, Appl. Phys. Lett. **109**, 252402 (2016).

[2] T. Chen, R. K. Dumas, A. Eklund, P. K. Muduli, A. Houshang, A. A. Awad, P. Dürrenfeld, B. G. Malm, A. Rusu, and J. Çžkerman, Spin-torque and Spin-Hall nano-oscillators, Proc. IEEE **104**, 1919 (2016).

[3] H. S. Cho, S. Y. Kang, S. J. Cho, I.-Y. Oh, M. Shin, H. Park, C. Jang, B.-C. Min, S.-I. Kim, S.-Y. Park, and C. S. Park, Spin nano–oscillator–based wireless communication, Sci. Rep. **4**, 5486 (2014).

[4] R. Sharma, P. Dürrenfeld, M. Ranjbar, R. K. Dumas, J. Akerman, and P. K. Muduli, Modulation rate study in a spin-torque oscillator-based wireless communication system, IEEE Trans. Magn. **51**, 1 (2015).

[5] A. Litvinenko, V. Iurchuk, P. Sethi, S. Louis, V. Tyberkevych, J. Li, A. Jenkins, R. Ferreira, B. Dieny, A. N. Slavin, and U. Ebels, Ultrafast sweep-tuned spectrum analyzer with temporal resolution based on a spin-torque nano-oscillator, Nano Lett. **20**, 6104 (2020).

[6] D. Markovic, N. Leroux, A. Mizrahi, J. Trastoy, V. Cros, P. Bortolotti, L. Martins, A. Jenkins, R. Ferreira, and J. Grollier, Detection of the Microwave Emission From a Spin-Torque Oscillator by a Spin Diode, Phys. Rev. Appl. **13**, 044050 (2020).

[7] A. S. Jenkins, L. S. E. Alvarez, P. P. Freitas, and R. Ferreira, Digital and analogue modulation and demodulation scheme using vortex-based spin torque nano-oscillators, Sci. Rep. **10**, 11181 (2020).

[8] J. C. Slonczewski, Current-driven excitation of magnetic multilayers, J. Magn. Magn. Mat. **159**, L1 (1996).

[9] A. Slavin and V. Tiberkevich, Nonlinear auto-oscillator theory of microwave generation by spin-polarized current, IEEE Trans. Magn. **45**, 1875 (2009).

[10] W. H. Rippard, M. R. Pufall, S. Kaka, T. J. Silva, S. E. Russek, and J. A. Katine, Injection Locking and Phase Control of Spin Transfer Nano-Oscillators, Phys. Rev. Lett. **95**, 067203 (2005).

[11] S. Urazhdin, P. Tabor, V. Tiberkevich, and A. Slavin, Fractional Synchronization of Spin-Torque Nano-Oscillators, Phys. Rev. Lett. **105**, 104101 (2010).

[12] M. Quinsat, J. F. Sierra, I. Firastrau, V. Tiberkevich, A. Slavin, D. Gusakova, L. D. Buda-Prejbeanu, M. Zarudniev, J.-P. Michel, U. Ebels, *et al.*, Injection locking of tunnel junction oscillators to a microwave current, Appl. Phys. Lett. **98**, 182503 (2011).

[13] R. Lebrun, A. Jenkins, A. Dussaux, N. Locatelli, S. Tsunegi, E. Grimaldi, H. Kubota, P. Bortolotti, K. Yakushiji, J. Grollier, A. Fukushima, S. Yuasa, and V. Cros, Understanding of Phase Noise Squeezing Under Fractional Synchronization of a Nonlinear Spin Transfer Vortex Oscillator, Phys. Rev. Lett. **115**, 017201 (2015).

[14] J. Hem, L. D. Buda-Prejbeanu, and U. Ebels, Power and phase dynamics of injection-locked spin torque nano-oscillators under conservative and dissipative driving signals, Phys. Rev. B **100**, 054414 (2019).

[15] M. Tortarolo, B. Lacoste, J. Hem, C. Dieudonné, M.-C. Cyrille, J. A. Katine, D. Mauri, A. Zeltser, L. D. Buda-Prejbeanu, and U. Ebels, Injection locking at 2f of spin torque oscillators under influence of thermal noise, Sci. Rep. **8**, 1728 (2018).

[16] M. R. Pufall, W. H. Rippard, S. Kaka, T. J. Silva, and S. E. Russek, Frequency modulation of spin-transfer oscillators, Appl. Phys. Lett. **86**, 082506 (2005).

[17] R. Ma, A. Purbawati, M. Kreissig, F. Protze, A. Ruiz-Calaforra, J. Hem, U. Ebels, and F. Ellinger, in *13th Conference on Ph.D. Research in Microelectronics and Electronics (PRIME)* (2017), pp. 1–4.

[18] P. K. Muduli, Y. Pogoryelov, S. Bonetti, G. Consolo, F. Mancoff, and J. Çžkerman, Nonlinear frequency and amplitude modulation of a nanocontact-based spin-torque oscillator, Phys. Rev. B **81**, 140408(R) (2010).

[19] M. Manfrini, T. Devolder, J.-V. Kim, P. Crozat, C. Chappert, W. Van Roy, and L. Lagae, Frequency shift keying in vortex-based spin torque oscillators, J. Appl. Phys. **109**, 083940 (2011).

[20] M. Quinsat, F. Garcia-Sanchez, A. S. Jenkins, V. S. Tiberkevich, A. N. Slavin, L. D. Buda-Prejbeanu, A. Zeltser, J. A. Katine, B. Dieny, M.-C. Cyrille, and U. Ebels, Modulation bandwidth of spin torque oscillators under current modulation, Appl. Phys. Lett. **105**, 152401 (2014).

[21] R. Sharma, N. Sisodia, E. Iacocca, A. A. Awad, J. Åkerman, and P. K. Muduli, A high-speed single sideband generator using a magnetic tunnel junction spin torque nano-oscillator, Sci. Rep. **7**, 13422 (2017).

[22] A. Ruiz-Calaforra, A. Purbawati, T. Brächer, J. Hem, C. Murapaka, E. Jimenez, D. Mauri, A. Zeltser, J. A. Katine, M.-C. Cyrille, L. D. Buda-Prejbeanu, and U. Ebels, Frequency shift keying by current modulation in a MTJ-based STNO with high data rate, Appl. Phys. Lett. **111**, 082401 (2017).

[23] M. Quinsat, D. Gusakova, J. F. Sierra, J. P. Michel, D. Houssameddine, B. Delaet, M.-C. Cyrille, U. Ebels, B. Dieny, L. D. Buda-Prejbeanu, J. A. Katine, D. Mauri, A. Zeltser, M. Prigent, J.-C. Nallatamby, and R. Sommet, Amplitude and phase noise of magnetic tunnel junction oscillators, Appl. Phys. Lett. **97**, 182507 (2010).

[24] E. Grimaldi, A. Dussaux, P. Bortolotti, J. Grollier, G. Pillet, A. Fukushima, H. Kubota, K. Yakushiji, S. Yuasa, and V. Cros, Response to noise of a vortex based spin transfer nano-oscillator, Phys. Rev. B **89**, 104404 (2014).

[25] M. Kreißig, R. Lebrun, F. Potze, K. J. Merazzo, J. Hem, L. Vila, M. C. Cyrille, F. Ellinger, V. Cros, U. Ebels, and P. Bortolotti, Vortex spin-torque oscillator stabilized by phase locked loop using integrated circuits, AIP Adv. **7**, 056653 (2017).

[26] S. Tamaru, H. Kubota, Y. Kay, F. Akio, and S. Yuasa, Analysis of phase noise in a spin torque oscillator stabilized by phase locked loop, Appl. Phys. Expr. **9**, 053005 (2016).

[27] A. Balanov, N. Janson, D. Postnov, and O. Sosnovtseva, *Synchronization: From Simple to Complex* (Springer Science & Business Media, Berlin, 2008), ISBN 978-3-540-72128-4

[28] A. Pikovsky, M. Rosenblum, and J. Kurths, *Synchronization: a Universal Concept in Nonlinear Sciences*, vol. 12 (Cambridge University Press, New York, 2003).

[29] G. V. Osipov, J. Kurths, and C. Zhou, *Synchronization in Oscillatory Networks* (Springer Science & Business Media, Berlin, 2007), ISBN.

[30] Y. Zhou, J. Persson, and J. Akerman, Intrinsic phase shift between a spin torque oscillator and an alternating current, J. Appl. Phys. **101**, 09A510 (2007).

[31] A. Purbawati, F. Garcia-Sanchez, L. D. Buda-Prejbeanu, and U. Ebels, Enhanced modulation rates via field modulation in spin torque nano-oscillators, Appl. Phys. Lett. **108**, 122402 (2016).

[32] J. V. Kim, V. Tiberkevich, and A. N. Slavin, Generation Linewidth of an Auto-Oscillator with a Nonlinear

Frequency Shift: Spin-Torque Nano-Oscillator, Phys. Rev. Lett. **100**, 017207 (2008).

[33] Y. Zhou, V. Tiberkevich, G. Consolo, E. Iacocca, B. Azzerboni, A. Slavin, and J. Çžkerman, Oscillatory transient regime in the forced dynamics of a nonlinear auto oscillator, Phys. Rev. B **82**, 012408 (2010).

[34] Rafael Microelectronics, Inc, *R820T. High Performance Low Power Advanced Digital TV Silicon Tuner* (Datasheet, HsinChu, 2011).

[35] Freeware software defined radio program. http://airspy.com/download/. Accessed: 2019-05-28.

[36] See the Supplemental Material at http://link.aps.org/supplemental/10.1103/PhysRevApplied.16.024048 for the derivation of expressions for SNR, BER, MDR, maximum achievable distance of communication for a given power level, and channel bandwidth and a video of voice transmission.

[37] H. T. Friis, A note on a simple transmission formula, Proc. IRE **34**, 254 (1946).

[38] J. C. Webster, Interpretations of speech and noise characteristics of NTID learning centers, J. Acoust. Soc. Am. **66**, S37 (1979).

[39] L. Zeng, Y. Liu, H.-H. Chen, Y. Zhou, D. Zhang, Y. Zhang, and W. Zhao, Robust phase shift keying modulation method for spin torque nano-oscillator, Nanotechnology **31**, 375205 (2020).

[40] M. Zahedinejad, A. A. Awad, S. Muralidhar, R. Khymyn, H. Fulara, H. Mazraati, M. Dvornik, and J. Åkerman, Two-dimensional mutually synchronized spin Hall nano-oscillator arrays for neuromorphic computing, Nat. Nano **15**, 47 (2020).

[41] S. Tsunegi, T. Taniguchi, R. Lebrun, K. Yakushiji, V. Cros, J. Grollier, A. Fukushima, S. Yuasa, and H. Kubota, Scaling up electrically synchronized spin torque oscillator networks, Sci. Rep. **8**, 1 (2018).

[42] IEEE, The Institute of Electrical and Electronics Engineers, Inc. 3 Park Avenue, New York, NY 10016-5997, USA. Wireless LAN Medium Access Control (MAC) and Physical Layer (PHY) specifications (2003).